# Supersymmetric subelectroweak scale dark matter, the Galactic Center gamma-ray excess, and exotic decays of the 125 GeV Higgs boson

Jinrui Huang,[1,*] Tao Liu,[2,†] Lian-Tao Wang,[3,4,‡] and Felix Yu[5,§]

[1]*Theoretical Division, T-2, MS B285, Los Alamos National Laboratory, Los Alamos, New Mexico 87545, USA*

[2]*Department of Physics, The Hong Kong University of Science and Technology, Clear Water Bay, Kowloon, Hong Kong*

[3]*Enrico Fermi Institute, University of Chicago, Chicago, Illinois 60637, USA*

[4]*KICP and Department of Physics, University of Chicago, 5640 S. Ellis Avenue, Chicago, Illinois 60637, USA*

[5]*Theoretical Physics Department, Fermi National Accelerator Laboratory, P. O. Box 500, Batavia, Illinois 60510, USA*

(Received 23 July 2014; published 5 December 2014)

We continue our exploration of the nearly Peccei-Quinn symmetric limit shared by common singlet extensions of the minimal supersymmetric standard model. This limit has been established as a viable framework for studying subelectroweak scale dark matter phenomenology and has interesting and direct connections to new exotic Higgs decay physics. We present analytic calculations to motivate the important phenomenological features mentioned above. We also discuss benchmark points in this model framework that accommodate the observed Galactic center gamma-ray excess. We emphasize connections between phenomenology of dark matter direct detection and indirect detection, and new exotic decay channels for the 125 GeV Higgs boson. We conclude by identifying two benchmark modes of exotic Higgs decays for $h \to \tau^+\tau^- \not{E}_T$ and $h \to b\bar{b}\not{E}_T$ final states and estimate their sensitivity prospects at the LHC.

DOI: 10.1103/PhysRevD.90.115006 PACS numbers: 12.60.Jv, 14.80.Bn, 14.80.Da, 95.35.+d

## I. INTRODUCTION

As presented in two Letters [1,2], the Peccei-Quinn symmetry limit of singlet extensions of the minimal supersymmetric standard model (MSSM) encompasses rich Higgs and dark matter (DM) physics, whose phenomenology and collider signatures we began exploring in [1]. The singlet extensions, like the next-to-MSSM (NMSSM) [3] and nearly MSSM (nMSSM) [4], are traditionally motivated as possible solutions to the notorious $\mu$ problem in the MSSM and give rise to some limited scenarios for exotic Higgs decays and DM phenomenology. It was remarked, however, that these scenarios share a Peccei-Quinn (PQ) symmetry limit (cf. Ref. [5]), giving rise to novel Higgs and DM signatures outside the scope of previous studies.

Most notably, the PQ symmetry limit provides a supersymmetric framework for studying subelectroweak (sub-EW) scale DM [2]. Possibilities for sub-EW scale DM in typical MSSM contexts were stymied by LEP constraints and acceptable relic density requirements [6]. Having a sub-EW DM particle, however, neatly dovetails with exciting opportunities in Higgs physics, as the 125 GeV Higgs discovered by CMS [7] and ATLAS [8] has new exotic decay channels available. This connection between DM physics and exotic Higgs decays in the PQ symmetry limit scenario was explicitly explored in Ref. [1] for two benchmark models that gave rise to two distinct exotic Higgs signatures of $\mu^+\mu^-\not{E}_T$ and $b\bar{b}\not{E}_T$ from the 125 GeV Higgs decay. In this work, we will continue exploring this connection between DM physics and Higgs collider phenomenology with two new benchmarks. The first, which will give the exotic Higgs decay channel $\tau^+\tau^-\not{E}_T$, will help complete the set of possible observable or theoretically well-motivated decay modes for the 125 Higgs boson. The second will be a new benchmark corresponding to the $b\bar{b}\not{E}_T$ exotic decay, which instead of being optimized for discovery at the LHC, would instead be motivated as a possible model explaining the Galatic center gamma-ray excess [9–16]. Other discussions of models and associated phenomenology for the Galactic center (GC) gamma-ray excess include Refs. [17–43], although some interesting non-DM explanations are discussed in Refs. [44,45].

We will first review the phenomenology of the PQ-axion supermultiplet and the nearly PQ-symmetry limit of the NMSSM and nMSSM in Sec. II, which includes the sub-EW scale dark matter physics in this scenario, with bounds from both direct detection experiments and the parameter space favored by the GC gamma-ray excess covered, as well as its potential connection to exotic decays of the 125 GeV Higgs boson. In Sec. III, we detail our LHC search strategies for the separate channels of $h_2 \to \tau^+\tau^- + \not{E}_T$ and

*jinruih@lanl.gov
†taoliu@ust.hk
‡liantaow@uchicago.edu
§felixyu@fnal.gov

 © 2014 American Physical Society

$h_2 \to b\bar{b} + \not{E}_{\rm T}$. We conclude in Sec. IV. Detailed calculations of the mass eigenvalues and eigenstates of the $CP$-even Higgs sectors in the PQ-symmetry limit as well as the coupling $y_{h_2 a_1 a_1}$ are given in Appendixes A and B.

## II. PHENOMENOLOGY OF THE PECCEI-QUINN SYMMETRY LIMIT

As mentioned in Sec. I, the PQ symmetry limit of singlet extensions of the MSSM provides a supersymmetric context for studies of sub-EW scale DM and the corresponding exotic Higgs decays. In the PQ symmetry limit, the superpotential and soft supersymmetry-breaking terms are given by

$$\begin{aligned} \mathbf{W} &= \lambda \mathbf{S H_u H_d}, \\ V_{\rm soft} &= m_{H_d}^2 |H_d|^2 + m_{H_u}^2 |H_u|^2 + m_S^2 |S|^2 \\ &\quad - (\lambda A_\lambda H_u H_d S + \text{H.c.}), \end{aligned} \tag{1}$$

where $H_d$, $H_u$, and $S$ denote the neutral Higgs fields of the $\mathbf{H_d}$, $\mathbf{H_u}$, and $\mathbf{S}$ supermultiplets, respectively. We will temporarily ignore any possible explicit breaking of the PQ symmetry in Eq. (1), e.g. an NMSSM superpotential term $\kappa \mathbf{S}^3$, but we remark that such small terms are typically required in more realistic scenarios. In addition, we will further narrow our focus to the decoupling limit given by $\lambda = \frac{\mu}{v_S} \lesssim \mathcal{O}(0.1 - 0.3)$ ($\langle S \rangle = v_S$), which will simplify our analytic analysis as well as help avoid a Landau pole problem. We will also assume that there is no explicit $CP$ violation in the Higgs sector, since the current experimental data constrain large mixing between the $CP$-even and $CP$-odd Higgs states [46,47].

In this scenario, there are three important characteristics distinguishing it from typical MSSM or NMSSM-like scenarios, and we will discuss each in turn.

### A. The Peccei-Quinn axion supermultiplet

First, because of the PQ symmetry and supersymmetry (SUSY), there simultaneously coexist three particles of sub-EW scale: the gauge singletlike $CP$-even and $CP$-odd Higgs bosons, $h_1$ and $a_1$, and the singlinolike neutralino, $\chi_1$, with their masses much lighter than the scale of the PQ symmetry breaking and their phenomenology approximately model independent. These particles or mass eigenstates are strictly reduced to the PQ axion supermultiplet [saxion ($s$), axion ($a$), and axino ($\tilde{a}$)] in the SUSY limit.

The Goldstone (or PQ axion) supermultiplet is represented by

$$\mathbf{A} = A + \sqrt{2}\theta\tilde{a} + \theta^2 F_A, \qquad A = \frac{1}{\sqrt{2}}(s + ia) \tag{2}$$

after the PQ symmetry is spontaneously broken, where

$$\mathbf{A} = \sum_i \frac{q_i v_i}{v_{\rm PQ}} (\Sigma_{\mathbf{i}} - v_i), \tag{3}$$

in which $i = 1,2,3, v_i = \{v_S, v_u, v_d\}$, and $\Sigma_{\mathbf{i}} = \{\mathbf{S}, \mathbf{H_u}, \mathbf{H_d}\}$ are the superfields charged under the PQ symmetry with $\langle H_u \rangle = v_u$, $\langle H_d \rangle = v_d$, and $v = \sqrt{v_u^2 + v_d^2} = 174$ GeV. Here $v_{\rm PQ} = \sqrt{\sum_i q_i^2 v_i^2}$ is the $U(1)_{\rm PQ}$ breaking scale and $q_i$ is an effective $U(1)_{\rm PQ}$ charge of $\Sigma_{\mathbf{i}}$. In our model,

$$q_d = -q_S \sin^2\beta, \qquad q_u = -q_S \cos^2\beta, \tag{4}$$

and

$$v_{\rm PQ} = |q_S| \sqrt{v_S^2 + \frac{\sin^2 2\beta}{4} v^2}, \tag{5}$$

where $\tan\beta = v_u/v_d$. If $\Sigma_{\mathbf{i}}$ is not charged under any other continuous symmetries, then $q_i$ is simply its $U(1)_{\rm PQ}$ charge [48]. The axion ($a$) mass is protected by the Goldstone theorem, and it is related to the saxion ($s$) and axino ($\tilde{a}$) masses by SUSY. If the $U(1)_{\rm PQ}$ symmetry is global and SUSY is unbroken, then we have $m_s = m_{\tilde{a}} = m_a = 0$. If SUSY is broken (this is often true when $v_i \neq 0$), the saxion and axino become massive while the axion remains massless. There are two sources which may contribute to the mass splitting between the superfield components. The first arise as diagonal corrections in superspace. The second is the separate real scalar and fermion mixing with other massive particles. In the latter case, the mass eigenstates become misaligned with the original saxion and axino states. For $\lambda \lesssim 0.1$, $v_S$ is of TeV scale or above, since an EW scale $\mu$ is required by electroweak symmetry breaking (EWSB). This immediately leads to $v_{\rm PQ} \sim v_S \gg v$. The PQ symmetry breaking is then mainly controlled by the singlet superfield $\mathbf{S}$, and $\mathbf{A}$ is hence $\mathbf{S}$-like.

The diagonal axino mass at tree level is given by

$$m_{\tilde{a}} = \frac{-\sum_i q_i^2 v_i F_i}{v_{\rm PQ}^2}, \tag{6}$$

where $F_i$ is the $F$ component of the $i$th chiral supermultiplet which is charged under the $U(1)_{\rm PQ}$ symmetry. Note $m_{\tilde{a}}$ falls to zero when none of the PQ-charged $F$ terms obtain a vacuum expectation value [48]. Given

$$\begin{aligned} F_{\mathbf{H_d}} &= \lambda v_S v_u, \\ F_{\mathbf{H_u}} &= \lambda v_S v_d, \\ F_{\mathbf{S}} &= \lambda v_d v_u, \end{aligned} \tag{7}$$

we have

$$m_{\tilde{a}} = -\frac{\lambda^2 v^2 \sin 2\beta}{\mu} + \sum_i \mathcal{O}\left(\frac{\lambda^{5-i}}{\tan^i\beta}\right). \tag{8}$$

Since $v_{\rm PQ} \approx v_S \gg v$, the axino is mostly singlino in our case. The contribution to the axino mass from mixing with the gauginos is further suppressed by the product of $\lambda v/\mu \approx v/v_{\rm PQ}$ and a gauge coupling factor. An axino as light as $\mathcal{O}(10)$ GeV or even lighter is therefore quite natural in this context. We denote the axino and other neutralinos as $\chi_i$, with $\chi_1$ (mostly singlino) being the lightest. The largest nonsinglino content of $\chi_1$ is Higgsino, which is of the order $\lambda v/\mu$ and hence can be very small in our case. One important constraint on this scenario is the contribution of $Z \to \chi_1\chi_1$ to the $Z$ invisible decay width. In our case, the $Z\chi_1\chi_1$ coupling is suppressed by $(\lambda v/\mu)^2$, which is small in the decoupling limit since $\lambda \lesssim 0.1$ and $\mu \sim v$ [2]. At the same time, $Z \to \chi_1\chi_2$, if kinematically allowed, is only suppressed by $\lambda v/\mu$ and can be more constraining.

Next we consider the saxion mass, which has been discussed in detail in Refs. [2,49]. We briefly summarize the main conclusions here. At tree level, in the large $\tan\beta$ limit, the minimum of the scalar potential in our scenario satisfies

$$A_\lambda \approx \mu \tan\beta \gg m_Z. \tag{9}$$

For later convenience, we introduce two parameters

$$\varepsilon' = \frac{A_\lambda}{\mu \tan\beta} - 1, \qquad \varepsilon = \frac{\lambda\mu}{m_Z}\varepsilon', \tag{10}$$

which characterize the deviation from the exact relation in Eq. (9). After EWSB, the saxion mixes with two $CP$-even Higgses. We denote the lightest scalar as $h_1$. At tree level, we have

$$\begin{aligned}(m^2_{h_1})_{\rm tree} = &-4v^2\varepsilon^2 + 16\frac{v^4}{m_Z^2}\varepsilon^4 \\ &+ \frac{4\lambda^2 v^2}{\tan^2\beta}\left(1 - \frac{\varepsilon m_Z}{\lambda\mu}\right)\left(1 + \frac{2\varepsilon\mu}{\lambda m_Z}\right) \\ &+ \sum_i \mathcal{O}\left(\frac{\lambda^{5-i}}{\tan^i\beta}\right).\end{aligned} \tag{11}$$

We see that in the decoupling limit, $\lambda \ll 1$, $m_{h_1}$ can be much smaller than the EW scale without too much fine-tuning. At the same time, to avoid a tachyonic mass for $h_1$, there is an upper limit

$$\varepsilon^2 < \frac{\lambda^2}{\tan^2\beta}. \tag{12}$$

Based on these discussions, we would expect a natural coexistence of three light singlet or singlinolike particles, $h_1$, $a_1$, and $\chi_1$, in the PQ symmetry plus decoupling limit of singlet extensions of the MSSM. We also expect some small explicit PQ symmetry breaking which would generate a small mass for the axion, $a_1$. This feature is clearly shown in the NMSSM context in [2], while the lightness of $\chi_1$ in the PQ limit of the other MSSM extensions was also noticed in Refs. [50,51]. The light singlinolike $\chi_1$ provides a natural supersymmetric sub-EW scale DM candidate. In particular, the existence of light $a_1$ and $h_1$ states allow $\chi_1$ to achieve simultaneously the correct relic density and a spin-independent direct detection cross section varying over several orders, which is the focus of Sec. II B. We remark that this feature is absent in the $R$-symmetry limit of the NMSSM, where the coupling of the cubic term in superpotential $\kappa$ is large, leading to large contributions to the masses of both $m_{h_1}$ and $m_{\chi_1}$ at tree level.

### B. Sub-EW scale singlino DM

Second, if we assume $R$-parity conservation, $\chi_1$ can be a good DM candidate at the sub-EW scale, in contrast with usual MSSM constructions. The direct detection cross section for $\chi_1$ varies within a large range and arises dominantly via the exchange of a light scalar with nucleons. Moreover, the relic density is driven by pair annihilation of singlinolike neutralinos probing the light pseudoscalar resonance [2] and can match current measurements. While the correct DM relic density can also be achieved via an $s$-channel exchange of the singletlike $CP$-even Higgs boson, this process has no $s$-wave contribution and suffers a $p$-wave suppression: realistic scenarios typically require more fine-tuning, and the variability of the direct detection cross section is much more constrained for a given $m_{\chi_1}$.

In the past decade, motivated by a series of interesting direct detection experimental results (see [52–59]), many studies of sub-EW scale DM have been performed in various contexts (e.g. see [2,6,60]). It was found, however, that a strict MSSM context for sub-EW scale DM is not easy to achieve. Of the MSSM neutralinos, a winolike or Higgsino-like DM candidate would have an associated chargino at about the same mass and be ruled out from searches at LEP. A binolike DM candidate may be feasible, but it potentially requires the existence of extra light particles, such as sfermions, to mediate annihilation or coannihilation for reducing the DM relic density to an acceptable level, which has been generally excluded by SUSY searches at LEP and the LHC. These factors make sub-EW scale DM highly constrained in the MSSM (for more discussionsg, e.g. see [6]). In the singlet extensions of the MSSM, however, a light singlinolike neutralino, which generally arises in the nearly PQ-symmetry limit, is relatively unconstrained, and so the PQ-limit provides a supersymmetric benchmark to explore sub-EW scale DM phenomenology [2] (for some of the subsequent studies on DM physics in or related to this scenario, see [61]).

Sub-EW scale DM is now being revisited in the context of the GC gamma-ray excess [9–16] interpreted as an indirect detection of DM [9,11,12,14–43]. This gamma-ray excess was identified from data collected by the Fermi

Gamma Ray Space Telescope, and studies indicate the excess extends at least 10° from the GC, lessening the possibility of astrophysical fakes. Fits to the spectrum favor a roughly 30 GeV dark matter particle annihilating to $b\bar{b}$, with an annihilation cross section corresponding to that of a thermal relic, $\langle\sigma v_{\rm rel}\rangle = 3\times10^{-26}$ cm$^3$/s [9,11,12,14–17]. Again, this hint of sub-EW scale DM cannot be accommodated in the MSSM, but we will show a suitable benchmark in the PQ limit of singlet extensions of the MSSM.

In particular, the natural annihilation channel for 30 GeV singlinos in the PQ symmetry limit is via $\chi_1\chi_1 \to a_1 \to b\bar{b}$. For $m_{\chi_1}\sim 30$ GeV and $m_{a_1}\sim 60$ GeV, the $a_1$ pseudoscalar preferentially decays to the heaviest kinematically open pair of SM fermions, namely $b\bar{b}$. For the GC gamma-ray excess, this will serve to avoid diluting the gamma-ray spectrum shape.

The light $a_1$ and $h_1$ states are critical for helping $\chi_1$ achieve the appropriate relic density as well as determining the direct detection possibilities. Unlike an $s$-wave dominant annihilation process, the thermally averaged annihilation cross section $\langle\sigma v_{\rm rel}\rangle$ is sensitive to the temperature for processes mediated by the Breit-Wigner enhancement effect, e.g. the one under consideration (for general discussions on the Breit-Wigner mechanism in DM physics, see [62,63]). This is simply because the chance for the annihilated DM particles to sit on or close to the mediator resonance is temperature dependent. For example, if $m_{a_1}$ is smaller than $2m_{\chi_1}$, as the temperature decreases, the annihilated DM particles get less active and hence have a better chance to sit close to the mediator resonance or have a larger $\langle\sigma v_{\rm rel}\rangle$. Explaining the GC gamma rays requires $\langle\sigma v_{\rm rel}\rangle\sim 10^{-26}$ cm$^3$/s. This means that $\langle\sigma v_{\rm rel}\rangle$ is smaller than this value in the early universe and the DM particles therefore are generically overproduced. So we will consider the case $m_{a_1} > 2m_{\chi_1}$ only. Different from the first case, $\langle\sigma v_{\rm rel}\rangle$ tends to have a larger value in the early Universe in this case (e.g. see [64]), leading to

$$\Omega h^2 \sim 10^{-4}\times\frac{0.5}{\mathrm{erfc}\left(\sqrt{\frac{m_{\chi_1}}{T_f}\left|1-\frac{m_{a_1}^2}{4m_{\chi_1}^2}\right|}\right)}. \tag{13}$$

To generate the observed DM relic density, therefore, new inputs like nonthermal production mechanisms are needed. This can be achieved by decaying thermally produced next-to-lightest supersymmetric particle (NLSP) (with its density before the decay denoted by $\Omega_{\rm NLSP}h^2$), such as slepton, sneutrino, or neutralino, with the DM relic density given by

$$\Omega h^2 = \frac{m_{\chi_1}}{m_{\rm NLSP}}\Omega_{\rm NLSP}h^2. \tag{14}$$

We will leave the detailed discussions of such mechanisms for future work.

### C. Exotic Higgs decays

The third main feature of the PQ symmetry limit is the set of new exotic decays for the SM-like Higgs boson, which can be potentially probed at colliders soon or in the future. We first note that in the PQ symmetry limit, unlike the $R$-symmetry limit, the exotic decay channels of the SM-like Higgs into a pair of light singletlike $CP$-even or $CP$-odd Higgs bosons are generically suppressed. The suppressed tree-level couplings of the SM-like Higgs boson $h_2$ with $h_1h_1$ and $a_1a_1$ can be directly calculated from the Higgs potential, given by [2]

$$\begin{aligned} y_{h_2a_1a_1} &= -\sqrt{2}\lambda\varepsilon\frac{m_Z v}{\mu}+\sum_i \mathcal{O}\left(\frac{\lambda^{4-i}}{\tan^i\beta}\right),\\ y_{h_2h_1h_1} &= -\sqrt{2}\lambda\varepsilon\frac{m_Z v}{\mu}+2\sqrt{2}\varepsilon^2 v+\sum_i \mathcal{O}\left(\frac{\lambda^{4-i}}{\tan^i\beta}\right) \end{aligned} \tag{15}$$

in the exact PQ limit. Here we have used the mixing parameters given in Eq. (A3) in Appendix A. Alternately, the coupling $y_{h_2a_1a_1}$ can be calculated using the properties of the Goldstone boson, which we detail in Appendix B. We see that both $\mathrm{Br}(h_2\to h_1h_1)$ and $\mathrm{Br}(h_2\to a_1a_1)$ are suppressed by $|\lambda\varepsilon|^2 \ll 1$. Therefore, these decay channels are rather inconsequential for the SM-like Higgs search in our scenario. This is different from the well-known physics in the $R$-symmetry limit of the NMSSM [65], where $a_1$ is light, playing a role of pseudo-Goldstone boson in breaking the approximate $R$ symmetry. There, the decay of the SM-like Higgs boson $h_2\to a_1a_1$ is typically significant.

The suppression of the $h_2\to h_1h_1, a_1a_1$ decay channels and the lightness of singlinolike $\chi_1$ in the PQ symmetry limit open up possibilities for a new category of exotic decays of the 125 GeV Higgs boson which are initiated by decay into two fermions [1]:

(i) if $\chi_2$ is binolike and satisfies $m_{\chi_2} < m_{h_2} - m_{\chi_1}$, then $h_2$ can decay significantly via $h_2\to\chi_1\chi_2$;

(ii) if $\chi_2$ is binolike and satisfies $m_{\chi_2} < \frac{m_{h_2}}{2}$, then $h_2$ can also decay significantly via $h_2\to\chi_2\chi_2$, though its branching ratio is relatively small, compared with $h_2\to\chi_1\chi_2$, due to the phase space suppression.

The binolike neutralino subsequently decays via the following main ways [1]:

(i) $\chi_2\to\chi_1 h_1/a_1\to\chi_1 f\bar{f}$, which is favored most by kinematics in general context, due to the lightness of $h_1/a_1$.

(ii) $\chi_2\to\chi_1 Z/Z^*\to\chi_1 f\bar{f}$, though this chain is strongly constrained by the availability of the phase space.

(iii) $\chi_2\to\chi_1\gamma$, whose branching ratio can be as large as $\mathcal{O}(0.01-0.1)$ in the case where the mass splitting between $\chi_1$ and $\chi_2$ is small, say, $m_{\chi_2}-m_{\chi_1} < m_{a_1/h_1}, m_Z$ [66].

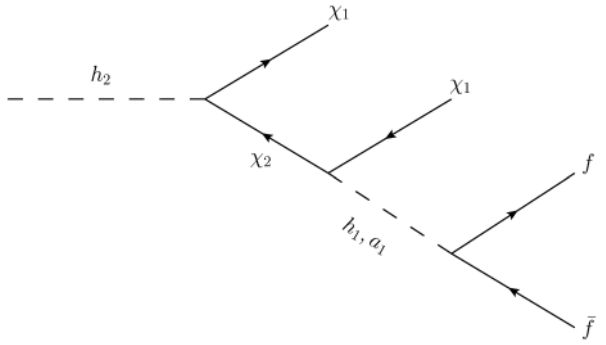


FIG. 1. A new decay channel for the SM-like Higgs boson, $h_2$, in the PQ-symmetry limit of the NMSSM.

The complete decay chain which is favored most by kinematics is shown in Fig. 1.[1] In addition, though it is not the focus of this article, if $m_{h_2} \lesssim m_{\chi_1} + m_{\chi_2}$, $h_2 \to \chi_1\chi_1$ can be significant. So, the decay topologies of $h_2$ in this scenario are very rich. As a matter of fact, for the seven possible topologies listed in Fig. 2 of Ref. [66], all of them can be achieved in this scenario except that the one $h_2 \to 2 \to 4$ is generically suppressed.

The richness of the $h_2$ decay topologies necessarily leads to variety of its kinematics at colliders. However, all of these decay chains eventually give a final state with at least one singlinolike $\chi_1$; the collider signatures therefore are generically semivisible (here we will not consider the possibility $h_2 \to \chi_1\chi_1$) or characterized by missing transverse energy (MET) and some visible objects, with or without a resonance. For example, we have

$$h_2 \to \not{E}_{\mathrm{T}} + b\bar{b}, \quad \tau^+\tau^-, \quad \ell^+\ell^-, \quad \gamma\gamma, \quad \gamma, \qquad (16)$$

for $h_2 \to \chi_1\chi_2$. The visible objects can be either collimated, via the decays of the light resonance $a_1/h_1$, or isolated, via the decays of the $Z$ boson. The discussion can be generalized to $h_2 \to \chi_2\chi_2$ though its final state is more complicated and the decay products tend to be softer. The sensitivity of the LHC to these possibilities is mainly driven by the final state signature. Here we will focus on the topology shown in Fig. 1, considering its novelty and its favoredness by kinematics.

For $h_1$, $a_1 \lesssim 1$ GeV, the corresponding decay $h_2 \to \mu^+\mu^-\not{E}_{\mathrm{T}}$ is easy to identify at the LHC with a specialized muon-jet identification procedure, which we detailed in [1] and has been highlighted as one of the highly motivated exotic Higgs searches within the 7 and 8 TeV data set of the LHC in Ref. [66]. For $1 \lesssim h_1$, $a_1 \lesssim 4$ GeV, the decay to strange mesons or a gluon pair is typically dominant [66]. They are very difficult to detect, and we do not expect that any sensitivity can be obtained with conventional cut and count analyses. But, potentially this parameter region can be still probed by $h_2 \to \mu^+\mu^-\not{E}_{\mathrm{T}}$ with a future data set from the LHC run II program, given $\mathrm{Br}(a_1 \to \mu^+\mu^-) \sim \mathcal{O}(0.01 - 0.1)$ for $\tan\beta > 1$ [66].

[1]This decay topology was also noted in a simplified model context [67].

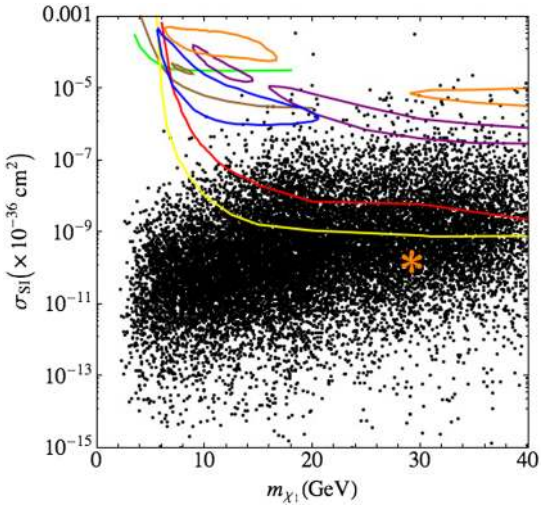


FIG. 2 (color online). Spin-independent direct detection cross section for $\chi_1$ in the nearly PQ-symmetry limit of the NMSSM. The scan is over all parameters, in the ranges $0.05 \le \lambda \le 0.3$, $0.0005 \le \kappa \le 0.03$, $|\varepsilon'| = |\frac{A_\lambda}{\mu \tan\beta} - 1| \le 0.25$, $-120 \le A_\kappa \le 0\,\mathrm{GeV}$, $5 \le \tan\beta \le 25$, and $100 \le \mu \le 400$ GeV. We have assumed soft squark masses of 2 TeV, slepton masses of 200 GeV, $A_{u,d,e} = -3.5$ TeV, and bino, wino, and gluino masses of 80–120, 200, and 2000 GeV, respectively. The black points have a relic density $\Omega h^2 \le 0.131$ (a default choice set in NMSSMTools 4.2.1 [69]). The curves show limits at 90% C.L. from the CDMSlite [52] (green, leftmost light line), updated XENON10 S2-only [53] (brown, leftmost dark line), XENON100 [54] (red, lowest dark line), and LUX [55] (yellow, lowest light line) analyses. The contours identify possible signal regions associated with data from CoGeNT [56] (brown, small, narrow dark contour, 90% C.L.), DAMA/LIBRA [57] (orange, topmost two light contours, 99.7% C.L.), CRESST [58] (purple, topmost two dark contours, 95.45% C.L.), and CDMS II Si [59] (blue, top-left large dark contour, 90% C.L) experiments. The orange star corresponds to the benchmark presented in Table I.

For $4 \lesssim h_1$, $a_1 \lesssim 10$ GeV, the decay to tau pairs and missing transverse energy can be potentially probed with large amounts of integrated luminosity, which we discuss in Sec. III A. For scalar and pseudoscalar masses larger than 10 GeV (and given the decay topology in Fig. 1), the dominant decay to $b\bar{b}$ is possible to probe at the LHC. We studied one discovery possibility in [1], but in Sec. III B, we will focus on a new benchmark motivated by the GC gamma-ray excess.

As a last comment in this section, we note that the monojet searches at the LHC (cf. [68]) generally have no sensitivity to this scenario, even if $\sigma_{\mathrm{SI}}$ is as large as $10^{-40}$ cm$^2$. This is because the singletlike mediator typically has a small production cross section and in addition, mainly decays into the SM fermions.

TABLE I. Benchmark of sub-EW DM in the nearly PQ-symmetry limit of the NMSSM which is dedicated to encoding the event excess of cosmic gamma ray from the GC. Soft SUSY-breaking sfermion and gaugino parameters are as given in the caption of Fig. 3. All mass parameters are in GeV, and $\sigma_{\rm SI}$ and $\langle\sigma v\rangle_{0K}$ have units of cm$^2$ and cm$^3$/s, respectively.

| $\lambda$ | $\kappa$ | $A_\lambda$ | $A_\kappa$ | $\mu$ | $\tan\beta$ | $m_{h_1}$ | $m_{a_1}$ | $m_{\chi_1}$ |
|---|---|---|---|---|---|---|---|---|
| 0.21 | 0.01 | 3047.2 | −78.0 | 307.8 | 10.0 | 21.9 | 58.9 | 29.4 |
| $m_{h_2}$ | $m_{\chi_2}$ | $\mathrm{Br}(h_2 \to \mathrm{SM})$ | $\mathrm{Br}(h_2 \to \chi_1\chi_2)$ | $\mathrm{Br}(\chi_2 \to \chi_1 h_1)$ | $\mathrm{Br}(h_1 \to b\bar{b})$ | $\Omega h^2(10^{-5})$ | $\sigma_{\rm SI}(10^{-46})$ | $\langle\sigma v\rangle_{0K}(10^{-26})$ |
| 125.0 | 80.9 | 75.0% | 18.5% | 100% | 86.7% | 8.0 | 1.7 | 2.5 |

### D. Parameter space scan

We can illustrate many of the features described in Secs. II A–II C with a general parameter space scan in the PQ symmetry limit of the NMSSM.

In Fig. 2, we show the current bounds of DM direct detections on this scenario, with the black points resulting in a relic density $\Omega h^2 \leq 0.131$ and satisfying all of the other built-in constraints in NMSSMTools 4.2.1 [69], such as from Higgs searches, superpartner searches, muon $g-2$, flavor physics, invisible $Z$-decay, and the constraints from $\Upsilon$ decays. The curves show limits at 90% C.L. from the CDMSlite [52] (green, leftmost light line), updated XENON10 S2-only [53] (brown, leftmost dark line), XENON100 [54] (red, lowest dark line), and LUX [55] (yellow, lowest light line) analyses. The contours identify possible signal regions associated with data from CoGeNT [56] (brown, small, narrow dark contour, 90% C.L.), DAMA/LIBRA [57] (orange, topmost two light contours, 99.7% C.L.), CRESST [58] (purple, topmost two dark contours, 95.45% C.L.), and CDMS II Si [59] (blue, top-left large dark contour, 90% C.L) experiments. The orange star corresponds to the benchmark presented in Table I. The unconstrained parameter space in this scenario can be readily probed by future iterations of current DM direct detection experiments.

In Fig. 3, we show physics in the neighborhood of the benchmark point (orange star) which is used to explain the GC gamma-ray excess. The panels in the top row show the simultaneous smallness of $m_{h_1}$, $m_{a_1}$, and $m_{\chi_1}$. The panels in the middle row show the relic density given by a pair annihilation enhanced by the $a_1$-mediated Breit-Wigner effect, as well as the thermally averaged annihilation cross section in the Universe nowadays. Indeed, one can find a narrow band where $\langle\sigma v\rangle_{0K} \sim 10^{-26}$ cm$^3$ s$^{-1}$. Yet, the overlap of this band with the correct $\Omega_{\chi_1}h^2$ is a very small slice of the parameter space. Obtaining the correct relic abundance requires a delicate fine-tuning of parameters if the annihilation mechanism through the $a_1$ pseudoscalar is the only avenue available, and indeed, the benchmark presented in Table I does not have an appropriate $\Omega_{\chi_1}h^2$ to saturate the DM relic density. As emphasized before, however, nonthermal production mechanisms of the DM can alleviate this problem and are, in fact, required for much of the parameter space. This can be satisfied by decays of thermally produced NLSPs, which put nontrivial constraints on the remaining sparticle spectrum outside of the exotic Higgs decay signatures. The cosmological constraints and limits from direct collider searches and indirect flavor observables on the required sparticle spectrum to nonthermally produce the $\chi_1$ DM is a discussion we will reserve for future work. Nonetheless, the panels in the last row indicate that, if $\chi_2$ is binolike and of the sub-EW scale, the decay of $h_2 \to \chi_1\chi_2$ is significant.

## III. EXOTIC HIGGS DECAYS SEARCH STRATEGIES AT THE LHC

We now focus on the possibilities for exotic decays of the SM-like Higgs boson that arise from the PQ-symmetry limit. As depicted in Fig. 1, we study the decay chain $h_2 \to \chi_1\chi_2$, with $\chi_2 \to \chi_1 h_1$, $\chi_1 a_1$, and $h_1$, $a_1 \to f\bar{f}$. For our benchmark scenario, the collider signature will be $f\bar{f} + \not{E}_{\rm T} + X$, where the SM fermions $f\bar{f}$ are produced via the decay of the light resonance $h_1$ or $a_1$ and appear as a pair of collimated leptons, jets, or merge into a fat jet at the LHC, and $X$ denotes the decay products of the particles produced in association with $h_2$. We have studied the cases with $f\bar{f} = \mu^+\mu^-$, $b\bar{b}$ in Ref. [1]. Here, we will extend our analysis to include the $\tau^+\tau^-$ final state as well as consider a modified benchmark for the $b\bar{b}$ channel that is motivated by the connection to the GC gamma-ray excess.

Similar to Ref. [1], we introduce a scale factor

$$c_{\rm eff} = \frac{\sigma(pp \to h_2)}{\sigma(pp \to h_{\rm SM})} \times \mathrm{Br}(h_2 \to \chi_1\chi_2) \times \mathrm{Br}(\chi_2 \to h_1\chi_1) \times \mathrm{Br}(h_1 \to f\bar{f}), \quad (17)$$

where $\sigma(pp \to h_2)$ and $\sigma(pp \to h_{\rm SM})$ are the production cross sections for the SM-like and SM Higgs boson (the first calculated in the PQ-symmetry limit of the NMSSM and the second calculated in the SM) in the relevant production mode, and we assume the narrow width approximation for each intermediate decaying particle. The current limits on an invisible or unobserved decay width for the Higgs boson are as large as 60% (25%) at the 95% C.L., with an enhanced $\Gamma(h_2 \to gg)$ allowed (not allowed) [70]. As the limit on a nonstandard Higgs decay width improves, our final sensitivity results can be rescaled by the $c_{\rm eff}$ factor, in the same spirit as the simplified model framework [71]. We also note that exotic production modes for the SM-like Higgs boson could increase the effective production rate [72]. The effective rate for our signal, however, not only derives from direct exotic decays of the

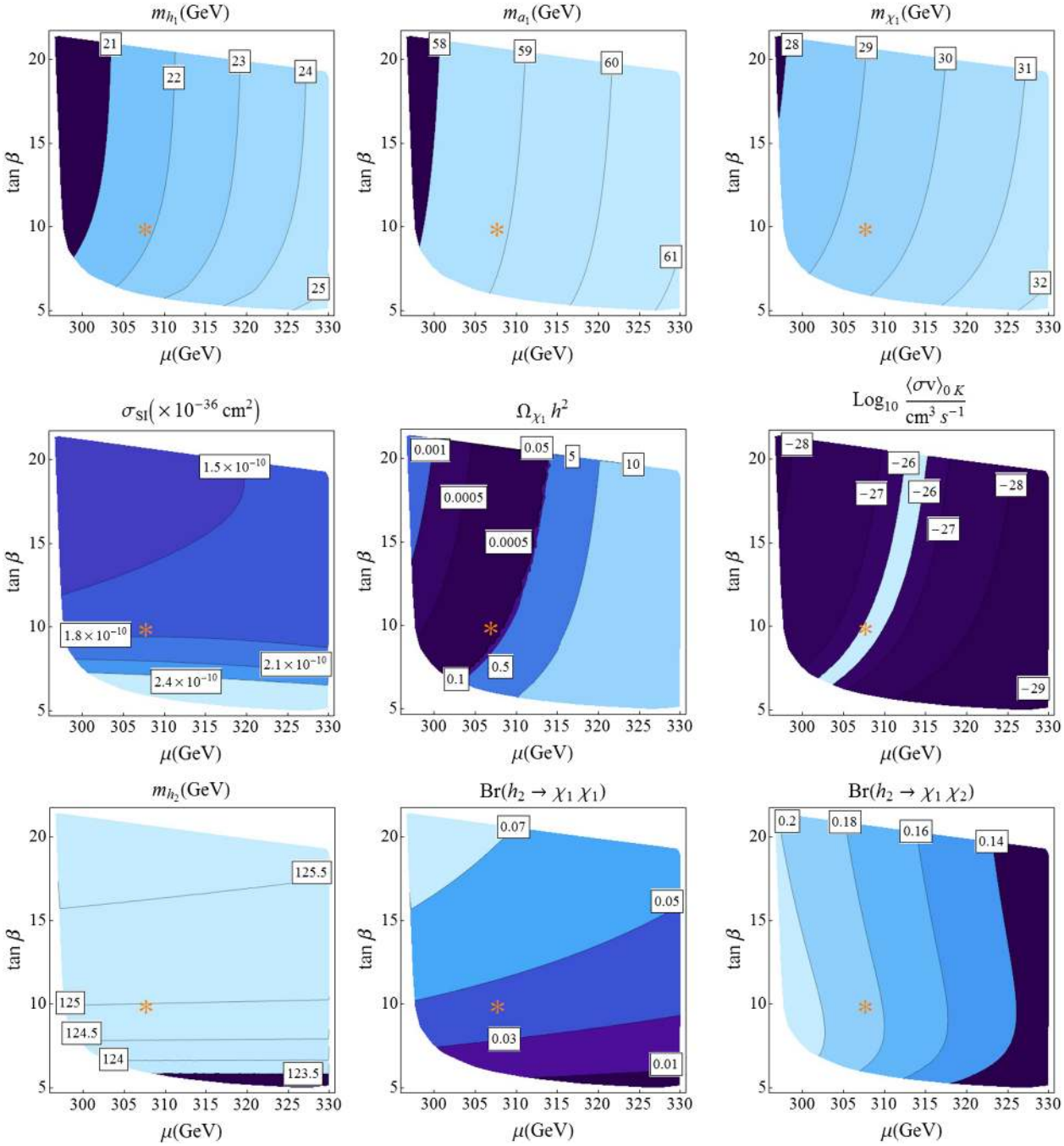


FIG. 3 (color online). Embedding the gamma-ray excess from the GC as DM signals in the nearly PQ-symmetry limit of the NMSSM. Here $\lambda = 0.21$, $\kappa \leq 0.01$, $\varepsilon' = -0.01$, and $A_\kappa = -78$ GeV have been assumed. In addition, soft SUSY-breaking parameters for gauginos, squarks, and sleptons are set to be $M_1 = 85$ GeV, $M_2 = 200$ GeV, $M_3 = 2000$ GeV, $\tilde{M}_l^2 = (200\ \mathrm{GeV})^2$, and $\tilde{M}_q^2 = (2000\ \mathrm{GeV})^2$, respectively; soft SUSY-breaking trilinear parameters are assumed to be $A_u = A_d = A_l = -3500$ GeV. The orange star represents the benchmark point shown in Table I.

SM-like Higgs but also alternates production modes of the light NMSSM resonances in our model. From Table I, we note that the binolike $\chi_2$ has a 100% branching fraction to $\chi_1 h_1$: this is reminiscent of gauge-mediation SUSY models with a light gravitino, where every SUSY cascade in our model ends with a $\chi_2$ NLSP that subsequently decays to $\chi_1 h_1$. Hence, the LHC prospects of discovering the signature of light NMSSM resonances could be greatly enhanced via non-Higgs exotic decays and not be constrained by global fits to the invisible or exotic decay branching fraction of the SM-like Higgs. Although our analyses are optimized for finding the light NMSSM

resonances via their kinematics as decay products of the SM-like Higgs, these additional modes would certainly improve the sensitivity prospects as long as the new sparticles are within the reach of the LHC. Hence, the $c_{\rm eff}$ scaling factor defined in Eq. (18) only captures a piece of the potential signal yield for $h_1 + \not{E}_{\rm T}$ production. Clearly, though, an optimized analysis of these additional modes would require a separate collider analysis, which we reserve for future work.

In our analyses, the signal and background samples for both analyses are simulated using MadGraph 5 [73] with CTEQ6L1 parton distribution functions [74] and MLM matching [75,76], with a matching scale $Q = 30$ GeV. The $h_2$ decays are handled in MadGraph 5 implementing an NMSSM model file based on Ref. [2]. These events are showered and hadronized using PYTHIA v6.4.20 [77]. Jet clustering is performed with the FASTJET v.3.0.2 [78] package. As with Ref. [1], we use a mock detector simulation incorporating ATLAS and CMS performance results on jets [79], electrons [80], muons [81], and missing energy [82].

### A. Case I: $h_2 \to \tau^+\tau^- + \not{E}_{\rm T}$

For $4 \lesssim m_{h_1} \lesssim 10$ GeV, the dominant decay of $h_1$ proceeds via two tau leptons. For concreteness, we adopt the benchmark indicated in Table II. Because of the small $h_1$ mass, the two taus are relatively soft and only obtain their boost from the kinematics of the cascade decay. So we adopt the SM Higgs production mode $Zh_2$, and we will trigger on $Z \to \ell^+\ell^-$, $\ell = e$ or $\mu$. The moderate boost to $h_2$ provided by the recoiling $Z$ combined with the available phase space from the cascade decay $h_2 \to \chi_2\chi_1, \chi_2 \to \chi_1 h_1$, $h_1 \to \tau^+\tau^-$ will serve to roughly collimate the ditau pair. We will focus on the tau decays characterized by one-prong and three-prong tracks, where the prongs include both charged pions as well as charged leptons. The alternate high $p_T$, isolated leptonic tau decays will likely be very difficult to identify because of the loss of statistics and the characteristic softness of the leptons. Then, the signal is characterized by an opposite-sign (OS), same-flavor (SF) dilepton $Z$ candidate, a jet with track counts consistent with tau parents, and missing transverse energy.

The SM backgrounds for this challenging signal are $Z +$ jets, $Z \to \ell^+\ell^-$, fully leptonic $t\bar{t}$, fully leptonic $W^+W^-$, fully leptonic $W^\pm Z$, and $ZZ \to \ell\ell\nu\nu$. For the electroweak $Z +$ jets and the diboson backgrounds, we adopt a flat $K$ factor of 1.3. The $t\bar{t}$ background is normalized to 833 pb at 14 TeV LHC [83] to account for next-to-leading order (NLO) + next-to-leading logarithm QCD corrections. The signal cross section for $Zh_2$ production was fixed to 0.9690 for $h_2$ 125 GeV [84], which includes next-to-next-to-leading order QCD + NLO EW corrections. We adopt $c_{\rm eff} = 1$, and our results can be readily rescaled for other values.

TABLE II. Benchmark used for the collider analysis of $h_2 \to \tau^+\tau^- + \not{E}_{\rm T}$.

| | $m_{h_1}$ | $m_{h_2}$ | $m_{\chi_1}$ | $m_{\chi_2}$ |
|---|---|---|---|---|
| $h_1 \to \tau^+\tau^-$ | 8 GeV | 125 GeV | 10 GeV | 80 GeV |

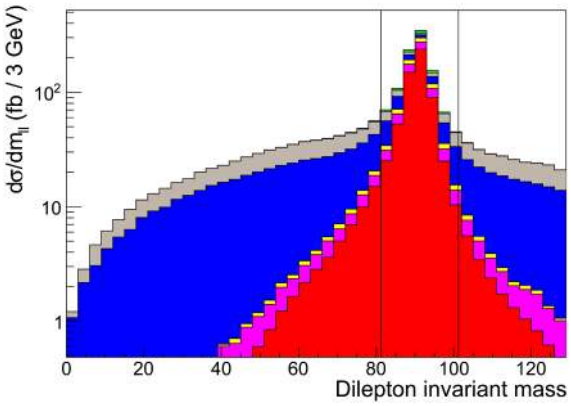


FIG. 4 (color online). Opposite-sign, same flavor lepton pair invariant mass distributions for the $h_1 \to \tau^+\tau^-$ signal benchmark (green), and $Z +$ jets $\times\, 1/500$ (red), $W^\pm Z$ (magenta), $ZZ$ (yellow), $t\bar{t} \times 1/10$ (blue), and $W^+W^-$ (gray) backgrounds. The signal is normalized using $c_{\rm eff} = 1$. The black vertical lines at 81.2 GeV and 101.2 GeV mark the dilepton mass window used in our analysis.

For efficient Monte Carlo generation, we apply preselection cuts to the backgrounds. Namely, we require at least one jet with $p_T > 30$ GeV and leptons have $p_T > 20$ GeV. The signal sample is without preselection requirements.

Events are clustered with the anti-$k_T$ algorithm using $R = 0.6$, which will serve as our candidate hadronic ditau signal jet. We select events with at least two leptons with $p_T > 20$ GeV and $|\eta| < 2.5$, excluding $1.37 < |\eta| < 1.52$ for electron candidates. The highest $p_T$ pair of leptons is

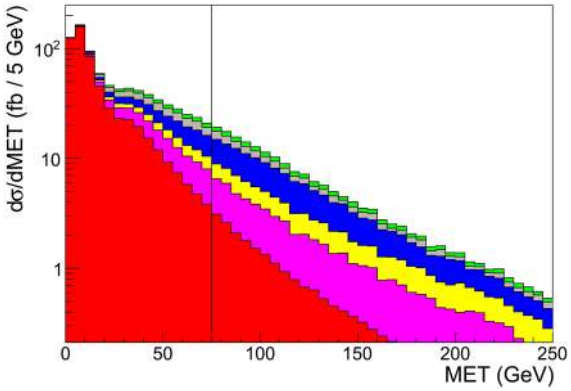


FIG. 5 (color online). MET distributions for the $h_1 \to \tau^+\tau^-$ signal benchmark (green), and $Z +$ jets $\times \frac{1}{500}$ (red), $W^\pm Z$ (magenta), $ZZ$ (yellow), $t\bar{t} \times \frac{1}{10}$ (blue), and $W^\pm W^\mp$ (gray) backgrounds. The signal is normalized using $c_{\rm eff} = 1$. The black vertical line at 75 GeV indicates our MET cut.

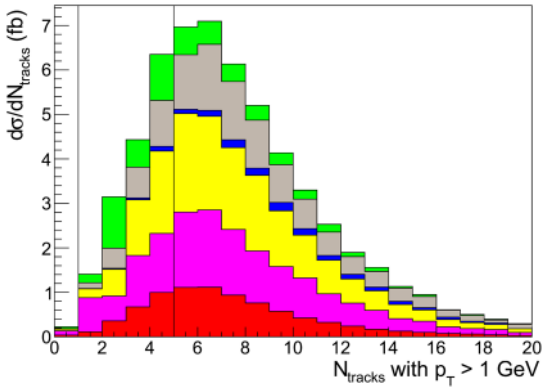


FIG. 6 (color online). Number of charged tracks with track $p_T > 1$ GeV for the $h_1 \to \tau^+\tau^-$ signal benchmark (green), and $Z + \text{jets} \times \frac{1}{500}$ (red), $W^\pm Z$ (magenta), $ZZ$ (yellow), $t\bar{t} \times \frac{1}{10}$ (blue), and $W^\pm W^\mp$ (gray) backgrounds. The signal is normalized using $c_{\text{eff}} = 1$. We count the number of events with 1 to 5 tracks, indicated by the black lines.

required to be the same flavor and opposite sign, and their invariant mass must fall within 10 GeV of the $Z$ mass. This helps reduce the nonresonant dilepton background from $t\bar{t}$ and $W^+W^-$, as evident in Fig. 4.

We next require $\not{E}_{\text{T}} > 75$ GeV, which helps reduce the $Z + \text{jets}$ background. Although the $Z + \text{jets}$ background has no intrinsic source for MET, our jet mismeasurement modeling leads to spurious MET signals. Also, as opposed to traditional SUSY pair production jets + MET searches, the mass scale for our hard process is not large, so the MET tail in our distribution is not highly pronounced; see Fig. 5. A future analysis in this channel would greatly benefit from improving the jet mismeasurement modeling and a possible subtraction of the $Z + \text{jets}$ background from the differential MET distribution.

We can readily eliminate much of the remaining $t\bar{t}$ background by vetoing $b$-tagged jets, where we adopt a $b$-tagging efficiency of 60% for $b$ jets, 10% for $c$ jets, and a 1% mistag rate. We isolate the $N_{\text{jet}} = 1$ bin and study the track content. From Fig. 6, we see that the signal characteristically has fewer hard tracks than the backgrounds, with prominent peaks at 2 and 4 tracks corresponding to the two one-prong and three-prong hadronic tau decays. We sum over 1 to 5 tracks in a moderately inclusive fashion to help avoid difficulties with track quality requirements. The cut efficiencies are listed in Table III.

After applying all selection cuts, we find the signal can be detected with $2\sigma$ expected exclusion sensitivity from 500 fb$^{-1}$ of LHC 14 TeV data, assuming $c_{\text{eff}} = 1$. For $c_{\text{eff}} = 0.5$, however, we expect the total HL-LHC luminosity of 3 ab$^{-1}$ would only have $2.4\sigma$ sensitivity. This result is mainly driven by the very large $Z + \text{jets}$ background, where the only effective cuts to reduce this background is our $\not{E}_{\text{T}} > 75$ GeV requirement and the track number cut. As mentioned before, the MET tail from the $Z + \text{jets}$ background arises from our modeling of jet mismeasurement, which should roughly reproduce the gross features of an experimental analysis. But a better understanding of the jet energy scale will help improve the modeling of the MET tail, likely leading to improved discovery and exclusion prospects. An extensive improvement on the track number requirement is certainly possible, but would realistically include additional handles to optimize low $p_T$ hadronic tau candidates in a high pileup environment. This type of analysis is beyond the scope of the current work, but we reserve such a study for future work.

In addition, considering traditional SUSY pair production modes that lead to $\chi_2$ intermediate states in the cascade would provide a second source of $h_1 \to \tau^+\tau^-$ signal events,

TABLE III. Cut flow table for $Zh_2$, $Z \to \ell^+\ell^-$, $h_2 \to \chi_1\chi_1\tau^+\tau^-$. Cross sections for backgrounds include preselection cuts of at least one jet with $p_T > 20$ GeV and leptons with $p_T > 20$ GeV. Leptons from decays of gauge bosons include $e$, $\mu$, and $\tau$.

| Cut and efficiencies | $Z + h_2$ $0.098 \times c_{\text{eff}}$ pb | $Z + \text{jets}$, $Z \to \ell\ell$ 593.4 pb | $t\bar{t} \to b\ell^+\nu\bar{b}\ell^-\nu$ 41.82 pb | $W^+W^- \to \ell^+\nu\ell^-\nu$ 2.412 pb | $W^\pm Z \to \ell^\pm\nu\ell^+\ell^-$ 0.3461 pb | $ZZ \to \ell^+\ell^-\nu\nu$ 0.1299 pb |
|---|---|---|---|---|---|---|
| At least two SF, OS leptons with $p_T > 20$ GeV, within $Z$ window | 0.4389 | 0.4950 | $3.161 \times 10^{-2}$ | $3.151 \times 10^{-2}$ | 0.3113 | 0.4977 |
| MET > 75 GeV | 0.1632 | $1.803 \times 10^{-2}$ | $1.544 \times 10^{-2}$ | $9.002 \times 10^{-3}$ | 0.1057 | 0.2269 |
| Require $N_{b\text{-tags}} = 0$, only one jet $p_T > 20$ GeV | $6.052 \times 10^{-2}$ | $7.046 \times 10^{-3}$ | $4.03 \times 10^{-4}$ | $4.729 \times 10^{-3}$ | $4.226 \times 10^{-2}$ | 0.1313 |
| Require 1–5 tracks with $p_T > 3$ GeV | $3.710 \times 10^{-2}$ | $2.739 \times 10^{-3}$ | $6.526 \times 10^{-5}$ | $1.464 \times 10^{-3}$ | $1.575 \times 10^{-2}$ | $4.712 \times 10^{-2}$ |
| Event Number (500 fb$^{-1}$, $c_{\text{eff}} = 1.0$) | 1800 | $8.10 \times 10^5$ | 1400 | 1800 | 2700 | 3100 |
| $S/\sqrt{S+B}$(500 fb$^{-1}$, $c_{\text{eff}} = 1.0$) | | $2.0\sigma$ | | | | |

TABLE IV. Benchmark used for the collider analysis of $h_2 \to b\bar{b} + \not{E}_{\rm T}$.

| | $m_{h_1}$ | $m_{h_2}$ | $m_{\chi_1}$ | $m_{\chi_2}$ |
|---|---|---|---|---|
| $h_1 \to b\bar{b}$ | 20 GeV | 125 GeV | 30 GeV | 80 GeV |

where the more energetic kinematics would serve as a stronger handle against the backgrounds and also lead to improved prospects. As mentioned earlier, such production modes could also effectively enable signal rates to be uncorrelated with the potential improvement in the invisible and undetected branching fraction of the Higgs, which we parametrize by $c_{\rm eff}$.

### B. Case II: $h_2 \to b\bar{b} + \not{E}_{\rm T}$

For $m_{h_1} > 10$ GeV, the light Higgs-like scalar dominantly decays to $b\bar{b}$. As we are motivated by considering a possible model for the GC gamma-ray excess, we have adopted a benchmark point consistent with the parameter space scan presented in Sec. II B, which is listed in Table IV. This also contrasts with our previous study in Ref. [1], where the $h_1$ mass was much higher and hence easier to identify from the continuum $Z+$ heavy flavor jets background. In this case, the $h_1$ mass is 20 GeV, leading to a relatively soft $b\bar{b}$ pair. The event signature from the $h_2$ cascade is then $b\bar{b} + \not{E}_{\rm T}$. Since the $\not{E}_{\rm T}$ signature is only present to the extent that the $b\bar{b}$ system recoils, we again need a hard object for $h_2$ to recoil against as a useful trigger and to enhance the MET significance. For these purposes, we adopt the $Zh_2$ production mode, with $Z \to \ell^+\ell^-$, with $\ell = e$ or $\mu$. The signal is then a dilepton $Z$ candidate, a relatively soft $b$-tagged jet, and $\not{E}_{\rm T}$.

The main backgrounds for our signal are $Z+$ heavy flavor jets, including $Zg$, $g \to b\bar{b}$, $g \to c\bar{c}$, and $Zc + Z\bar{c}$ production, and $t\bar{t}$. We adopt 60% for our $b$-tagging efficiency, 10% for charm mistagging, and 1% for the remaining light flavor jet mistagging. While our dominant background will be from $Zg$ with gluon splitting to two $b$ quarks, there is still a non-negligible background from the charm-mistag background.

After our mild preselection requirements,[2] the starting cross sections at $\sqrt{s} = 14$ TeV LHC are 48.4 pb for $Zb\bar{b}$, 32.8 pb for $Zc\bar{c}$, 138.9 pb for $Zc + Z\bar{c}$, with subsequent $Z \to e^+e^-$, $\mu^+\mu^-$, or $\tau^+\tau^-$ decay, 41.8 pb for $t\bar{t}+$ jets, requiring the fully leptonic decays of the tops, and $0.098 \times c_{\rm eff}$ pb for our $Zh_2$ signal, again requiring $Z \to e^+e^-$, $\mu^+\mu^-$, or $\tau^+\tau^-$. The $t\bar{t}$ and signal cross sections are normalized the same as with the $\tau^+\tau^-$ analysis. Events are clustered with the angular-ordered Cambridge-Aachen algorithm [85,86] with distance parameter $R = 1.2$, in order to capture the larger $b\bar{b}$ system.

[2]We adopt the typical default requirements set in MadGraph 5 except for the $Z + g$ background, and we require the leptonic decay products of the $Z$ to have $p_T > 30$ GeV.

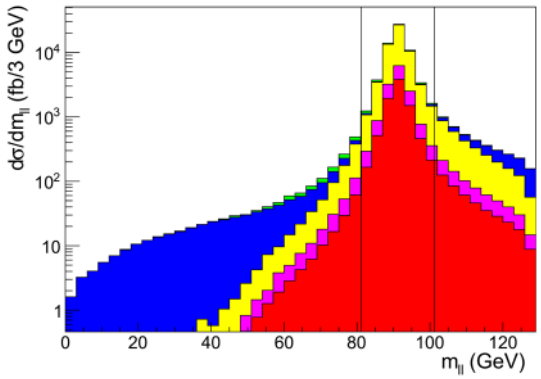


FIG. 7 (color online). Differential cross section vs $m_{\ell\ell}$ of same flavor, opposite sign lepton pairs for signal × 200 (green), $Zb\bar{b}$ background (red), $Zc\bar{c}$ background (magenta), $Zc, Z\bar{c}$ background (yellow), and $t\bar{t}$ background (blue) for the 14 TeV LHC. The black vertical lines indicate the mass window cut used requiring $81.2 < m_{ll} < 101.2$ GeV. We have set $c_{\rm eff} = 0.5$ for this channel.

We again start by identifying the leptonic $Z$ candidate, where the hardest dilepton pair must be an $e^+e^-$ or $\mu^+\mu^-$ pair with each having $p_T > 40$ GeV and satisfying $81.2\ {\rm GeV} < m_{\ell\ell} < 101.2$ GeV. Again, this helps to eliminate the nonresonant dilepton background from $t\bar{t}$, as evident in Fig. 7.

We then require $\not{E}_{\rm T} > 120$ GeV. In contrast with the $\tau^+\tau^-$ case, the signal carries a longer and harder $\not{E}_{\rm T}$ tail (see Fig. 8) arising from the different mass splittings in the benchmark we adopted. This cut is effective at eliminating the $Z+$ heavy flavor jet backgrounds, but the remaining contributions from these backgrounds are difficult to control because their MET tail again arises from our jet energy smearing.

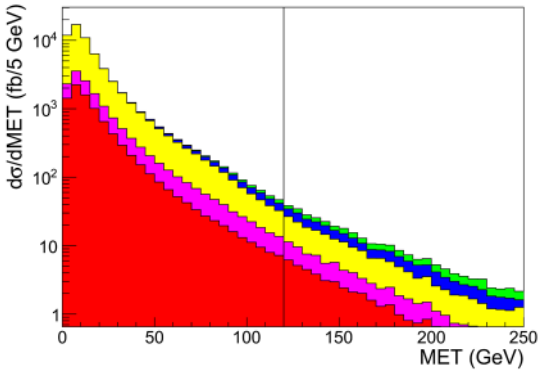


FIG. 8 (color online). Differential cross section vs MET for signal × 20 (green), $Zb\bar{b}$ background (red), $Zc\bar{c}$ background (magenta), $Zc, Z\bar{c}$ background (yellow), and $t\bar{t}$ background (blue) for the 14 TeV LHC after the $Z$ mass window cut. The black vertical lines indicate our MET > 120 GeV cut. We have set $c_{\rm eff} = 0.5$.

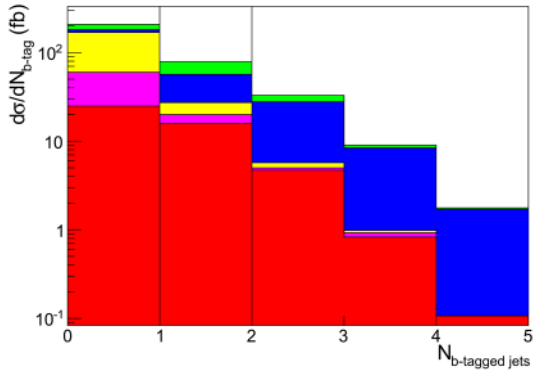


FIG. 9 (color online). Differential cross section vs $b$-tagged jet multiplicity for signal ×20 (green), $Zb\bar{b}$ background (red), $Zc\bar{c}$ background (magenta), $Zc, Z\bar{c}$ background (yellow), and $t\bar{t}$ background (blue), after the $Z$ mass window and MET cuts at the 14 TeV LHC. The black vertical lines indicate the required bin, $N_{b-\text{tags}} = 1$, used in our analysis. We have set $c_{\text{eff}} = 0.5$.

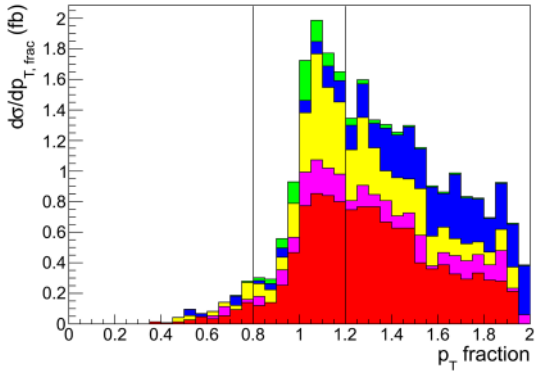


FIG. 10 (color online). Differential cross section vs $p_{T,\text{frac}}$, as defined in the text, for signal (green), $Zb\bar{b}$ background (red), $Zc\bar{c}$ background (magenta), $Zc, Z\bar{b}$ background (yellow), and $t\bar{t}$ background (blue), after applying the $Z$ mass window, MET, and $N_{b-\text{tag}} = 1$ cuts at the 14 TeV LHC. The black vertical lines indicate the $p_{T,\text{frac}}$ window, $0.8 < p_{T,\text{frac}} < 1.2$, requirement in our analysis. We have set $c_{\text{eff}} = 0.5$.

We now count the number of $b$-tagged jets with $p_T > 20$ GeV. Since the signal is best identified when its two bottom quarks are clustered into the same jet, as evident in Fig. 9, we retain the 1 $b$-tag bin and discard events with 0 or $\geq 2$ $b$-tagged jets.

Having isolated the dilepton system as well as the cascade decay of the $h_2$ boson, we can apply an additional cut with the expectation that the dilepton system recoils against the collimated $h_2$ cascade decay. We construct the scalar sum $p_T$ of the $h_2$ candidate, $p_T(h_2, \text{cand}) = p_T(b\text{-jet}) + |\not{E}_{\text{T}}|$, and then divide it by the $p_T$ of the dilepton system: $p_{T,\text{frac}} \equiv p_T(h_{2,\text{cand}})/p_T(\ell\ell_{\text{sys}})$. Shown in Fig. 10 is the distribution of the transverse momentum fraction, $p_{T,\text{frac}} \equiv p_T(h_{2,\text{cand}})/p_T(\ell\ell_{\text{sys}})$. We observe that the cutting on $p_{T,\text{frac}}$ works well at reducing the $t\bar{t}$ background, where the MET signal tends to arise from neutrinos of separate decay chains instead of a single cascade decay. We require $0.8 < p_{T,\text{frac}} < 1.2$ to isolate well-balanced $Zh_2$ candidate events.

After these cuts, we find that we have $2.0\sigma$ exclusion sensitivity with 50 fb$^{-1}$ of 14 TeV LHC luminosity. For $c_{\text{eff}} = 0.1$, which is the expectation for the ultimate sensitivity of the LHC to an exotic decay mode of the SM-like Higgs via coupling fits [66], we estimate that about 1.2 ab$^{-1}$ of 14 TeV LHC luminosity is required for $2.0\sigma$ sensitivity, although this luminosity scaling does not include any estimation of systematic effects. Complete cut flow information and sensitivity calculation are presented in Table V. The dominant background is from $Zb\bar{b}$, which could be further reduced with a grooming procedure looking for hard subjets if the signal were further on the $b\bar{b}$ continuum tail, as demonstrated in [1]. For our current benchmark, however, the lighter $h_1$ mass and the softer subjets render the grooming procedure ineffective at resolving the signal from the continuum background. Alternative jet substructure techniques, however, could be promising tools to resolve the $h_1 \to b\bar{b}$ signal bump, but additional handles on issues like subjet resolution and pileup mitigation would also need to be taken into account. As with the $h_1 \to \tau^+\tau^-$ scenario, further improvements could be made by studying traditional pair production modes of supersymmetric particles. The possibility of identifying single jets with multiple displaced vertices, corresponding to multiple $b$-hadron candidates, would also be a promising avenue for signal

TABLE V. Cut flow: Analysis cuts and efficiency table for the $h_1 \to b\bar{b}$ channel, $m_{h_1} = 20$, $\chi_1 = 30$, $\chi_2 = 80$ GeV. The decays $Z \to \ell^+\ell^-$ and $W \to \ell\nu$, $\ell = e, \mu, \tau$ are included in the quoted cross sections.

| Cut and efficiencies | $Zh_2$ $0.098 \times c_{\text{eff}}$ pb | $Zb\bar{b}$ 48.4 pb | $Zc\bar{c}$ 32.8 pb | $Zc + Z\bar{c}$ 138.9 pb | $t\bar{t}$ 41.8 pb |
|---|---|---|---|---|---|
| At least two SF, OS leptons with $p_T > 40$ GeV, within $Z$ window | 0.1946 | 0.1774 | 0.1707 | 0.1634 | 0.01193 |
| MET > 120 GeV | $5.547 \times 10^{-2}$ | $9.597 \times 10^{-4}$ | $1.205 \times 10^{-3}$ | $4.213 \times 10^{-4}$ | $1.765 \times 10^{-3}$ |
| $N_{b-\text{tags}} = 1$, jet $p_T > 20$ GeV | $2.303 \times 10^{-2}$ | $3.294 \times 10^{-4}$ | $1.231 \times 10^{-4}$ | $2.620 \times 10^{-5}$ | $7.058 \times 10^{-4}$ |
| $0.8 < p_{T,\text{frac}} < 1.2$ | $2.105 \times 10^{-2}$ | $1.935 \times 10^{-4}$ | $4.265 \times 10^{-5}$ | $1.160 \times 10^{-5}$ | $7.565 \times 10^{-4}$ |
| Event number (50 fb$^{-1}$, $c_{\text{eff}} = 0.5$) | 40 | 213 | 53 | 64 | 26 |
| $S/\sqrt{S+B}$(50 fb$^{-1}$, $c_{\text{eff}} = 0.5$) | | $2.0\sigma$ | | | |

extraction. We will leave these interesting questions for future work.

## IV. CONCLUSIONS

In this article, we emphasized that the nearly PQ-symmetry limit provides a supersymmetric benchmark for both a singlinolike sub-EW scale DM, as well as novel exotic decays of SM-like Higgs, $h_2 \to \chi_1\chi_2$ and $h_2 \to \chi_2\chi_2$, with the binolike $\chi_2$ further decaying in multiple ways. The collider signature of this new category of exotic Higgs decays is characterized by MET and some visible objects, with or without a resonance. We have pursued the $h_2 \to \chi_1\chi_2 \to h_1/a_1\chi_1\chi_1$ mode, which is favored more by kinematics, and presented analyses of the $\tau^+\tau^-$ and $b\bar{b}$ channels for extracting these signals from the SM backgrounds.

In the first analysis, we studied a benchmark model with $m_{h_1}=8\text{GeV}$, $m_{\chi_1}=10\text{GeV}$, and the decay $h_2 \to \tau^+\tau^- \not{E}_{\text{T}}$, where we adopted a track-based identification of pair of hadronic taus decays. We motivated the $Zh_2$, $Z \to \ell^+\ell^-$ production mode as the easiest trigger path, but nevertheless the relatively moderate MET from our signal implies the very large background from $Z+\text{jets}$ cannot be dramatically reduced. We estimate that roughly 500 $\text{fb}^{-1}$ of 14 TeV LHC luminosity is required to have $2\sigma$ exclusion sensitivity to this channel. Improving this channel would require new kinematic handles or alternative $\tau$ decay channels.

In the second analysis, we studied a GC gamma-ray excess benchmark with $m_{h_1} = 20$ GeV, $m_{\chi_1} = 30$ GeV, and $h_1 \to b\bar{b}$. The $Zh_2$, $Z \to \ell^+\ell^-$ production mode again provided a good trigger path, and the effective $b$-tagging requirements and larger MET signature of our signal were significantly more effective at reducing SM backgrounds. Using $c_{\text{eff}} = 0.5$, we estimate that 50 $\text{fb}^{-1}$ of 14 TeV LHC luminosity is needed to reach $2\sigma$ exclusion sensitivity for this benchmark. As reiterated from [1], one novel cut used in this analysis took advantage of the fact that for the decay topology in Fig. 1, the MET arises only from the $h_2$ decay, in contrast to the usual MET signatures of pair-produced MSSM superpartners or SM $t\bar{t}$ background.

The possibilities other than the ones discussed here (e.g. $h_2 \to \chi_2\chi_1$ with different $\chi_2$ decay modes, as well as $h_2 \to \chi_2\chi_2$) can lead to collider signatures and kinematics requiring different analyses from those we have presented. Additional production modes, such as those arising from pair production of superpartners, are also promising probes for studying the singletlike $h_1$ and singlinolike $\chi_1$ states. We will leave these interesting topics for a future study.

## ACKNOWLEDGMENTS

We would like to thank Brock Tweedie, Patrick Draper, Michael Graesser, Joe Lykken, Adam Martin, Nausheen Shah, Jessie Shelton, Matt Strassler, and Carlos Wagner for useful discussions. T. L. is supported by his start-up fund at the Hong Kong University of Science and Technology. J. H. is supported by the DOE Office of Science and the LANL LDRD program. J. H. would also like to thank the University of Washington for hospitality, where part of the work was finished. L-T. W. is supported by the DOE Early Career Award under Grant No. DE-SC0003930. L-T. W. is also supported in part by the Kavli Institute for Cosmological Physics at the University of Chicago through NSF Grant No. PHY-1125897 and an endowment from the Kavli Foundation and its founder Fred Kavli. F. Y. would like to thank the Theoretical High Energy Physics group at Johannes Gutenberg Universität Mainz for their hospitality, where part of this work was completed. Fermilab is operated by the Fermi Research Alliance, LLC under Contract No. DE-AC02-07CH11359 with the U.S. Department of Energy. We also would like to acknowledge the hospitality of the Kavli Institute for Theoretical Physics and the Aspen Center for Physics, where part of this work was completed, and this research is supported in part by the National Science Foundation under Grant No. NSF PHY11-25915.

*Note added.*—While this article was in preparation, the papers by Han *et al.* [87] and by Cheung *et al.* [88] appeared, which partially overlap with this one in discussing the potential role of the nearly PQ-symmetry limit of the NMSSM, a supersymmetric benchmark for sub-EW scale singlinolike DM [2], in explaining the GC gamma-ray excess. A notable difference, however, is that we emphasize the connection between sub-EW scale DM and the exploration of semivisible exotic decays of the 125 GeV Higgs boson, MET+ visible, at colliders [1], while [87] is focused on the mechanisms to achieve correct relic density and [88] is dedicated to the study on explaining the GC gamma-ray excess in supersymmetric scenarios.

## APPENDIX A: MASS EIGENVALUES AND EIGENSTATES OF THE *CP*-EVEN HIGGS SECTOR IN THE PQ LIMIT

The mass eigenvalues of the $CP$-even Higgs sector in the Peccei-Quinn limit are given by

$$\begin{aligned}
m_{h_1}^2 &= -\frac{4(\lambda^2 v^2 \mu^2 \varepsilon'^2)}{m_Z^2} \\
&\quad + \frac{4\lambda^2 v^2}{m_Z^6}\left(4v^2\varepsilon'^4\lambda^2\mu^4 + \frac{m_Z^4(1-\varepsilon')(m_Z^2+2\varepsilon'\mu^2)}{\tan^2\beta}\right) \\
&\quad + \sum_i \mathcal{O}\left(\frac{\lambda^{5-i}}{\tan^i\beta}\right), \\
m_{h_2}^2 &= m_Z^2 + \left(\frac{-4m_Z^2}{\tan^2\beta} + \frac{4v^2\varepsilon'^2\lambda^2\mu^2}{m_Z^2}\right) + \sum_i \mathcal{O}\left(\frac{\lambda^{3-i}}{\tan^i\beta}\right), \\
m_{h_3}^2 &= (1+\varepsilon')\mu^2\tan^2\beta + (1+\varepsilon')\mu^2 \\
&\quad + \left(\frac{3m_Z^2}{\tan^2\beta} + v^2(1+\varepsilon')\lambda^2\right) + \sum_i \mathcal{O}\left(\frac{\lambda^{3-i}}{\tan^i\beta}\right). \quad \text{(A1)}
\end{aligned}$$

In the extremal limit $\lambda = 0$, $m_{h_2}^2$ is reduced to

$$m_{h_2}^2 = m_Z^2 + \frac{-4m_Z^2}{\tan^2\beta} + \sum_i \mathcal{O}\left(\frac{\lambda^{3-i}}{\tan^i\beta}\right) = M_Z^2\cos^2 2\beta + \sum_i \mathcal{O}\left(\frac{\lambda^{3-i}}{\tan^i\beta}\right), \tag{A2}$$

a familiar result in the MSSM. The eigenstates of the three $CP$-even Higgs are given by

$$\begin{aligned}
S_{1d} &= \frac{\lambda v}{\tan\beta}\left(\frac{1}{\mu} + \frac{2\varepsilon'\mu}{m_Z^2}\right) + \sum_i \mathcal{O}\left(\frac{\lambda^{3-i}}{\tan^i\beta}\right),\\
S_{1u} &= \frac{2\ v\varepsilon'\lambda\mu}{m_Z^2} + \sum_i \mathcal{O}\left(\frac{\lambda^{3-i}}{\tan^i\beta}\right),\\
S_{1s} &= 1 + \sum_i \mathcal{O}\left(\frac{\lambda^{3-i}}{\tan^i\beta}\right),\\
S_{2d} &= \frac{1}{\tan\beta} + \sum_i \mathcal{O}\left(\frac{\lambda^{2-i}}{\tan^i\beta}\right),\\
S_{2u} &= 1 + \sum_i \mathcal{O}\left(\frac{\lambda^{2-i}}{\tan^i\beta}\right),\\
S_{2s} &= -\frac{2\lambda\varepsilon' v\mu}{m_Z^2} + \sum_i \mathcal{O}\left(\frac{\lambda^{2-i}}{\tan^i\beta}\right),\\
S_{3d} &= 1 + \sum_i \mathcal{O}\left(\frac{\lambda^{2-i}}{\tan^i\beta}\right),\\
S_{3u} &= -\frac{1}{\tan\beta} + \sum_i \mathcal{O}\left(\frac{\lambda^{2-i}}{\tan^i\beta}\right),\\
S_{3s} &= 0 + \sum_i \mathcal{O}\left(\frac{\lambda^{2-i}}{\tan^i\beta}\right).
\end{aligned} \tag{A3}$$

For our purposes, the eigenvalue and eigenstate of the lightest $CP$-even Higgs boson are calculated to an order above the other two.

## APPENDIX B: CALCULATION OF $y_{h_2a_1a_1}$

In this appendix, we calculate the coupling $y_{h_2a_1a_1}$ using the properties of the Goldstone boson. In the polar coordinates of the Higgs fields, $y_{h_2a_1a_1}$ arises from the kinetic term of $a_1$. We will take the kinetic term of $H_d$ as an illustration. We write $H_d$ as

$$H_d = \left(v_d + \frac{S_{1\,d}h_1 + S_{2\,d}h_2 + S_{3\,d}h_3}{\sqrt{2}}\right) \times \exp\left(\frac{i(P_{1\,d}a_1 + P_{2\,d}a_2 + P_{3\,d}a_3)}{v_d}\right). \tag{B1}$$

The relevant term in the $H_d$ kinetic term expansion is

$$\partial H_d^*\partial H_d \sim \sqrt{2}\frac{S_{2\,d}P_{1\,d}^2}{v_d}h_2\partial a_1\partial a_1. \tag{B2}$$

Because $a_1$ is massless, we have $\partial a_1\partial a_1 = p_{a_1}^2 a_1^2 = \frac{m_{h_2}^2}{2} = \frac{m_Z^2}{2} + \sum_i \mathcal{O}(\lambda^{2-i}/\tan^i\beta)$. So the contribution of the $H_d$ kinetic term to the $y_{h_2a_1a_1}$ is

$$\frac{S_{2\,d}m_{h_2}^2P_{1\,d}^2}{\sqrt{2}v_d}. \tag{B3}$$

With all Higgs kinetic terms incorporated, we have

$$y_{h_2a_1a_1} = \frac{m_Z^2}{\sqrt{2}}\left(\frac{S_{2\,d}m_{h_2}^2P_{1\,d}^2}{v_d} + \frac{S_{2\,u}m_{h_2}^2P_{1\,u}^2}{v_u} + \frac{S_{2\,s}m_{h_2}^2P_{1\,s}^2}{v_S}\right). \tag{B4}$$

with $P_{1\,d,1\,u,1\,s}$ defined in Eqs. (3)–(5) after decomposing the superfields and isolating into pseudoscalar components. This immediately reproduces Eq. (15).

## APPENDIX C: FURTHER DISCUSSION OF THE SAXION MASS

Unlike the axino, the saxion may obtain sizable mass corrections in its diagonal mass term or via its mixing with other massive particles, with SUSY softly broken. The diagonal saxion mass at tree level is given by

$$m_s^2 = \sum_{i,j}\frac{q_iv_i}{v_{\rm PQ}}M_{ij}\frac{q_jv_j}{v_{\rm PQ}} \tag{C1}$$

with

$$M_{ij} = \frac{\partial^2 V}{\partial\phi_i\partial\phi_j} + \frac{\partial^2 V}{\partial\phi_i^*\partial\phi_j}\bigg|_{\phi_{i,j},\phi_{i,j}^*=v_{i,j}} \tag{C2}$$

being the squared mass matrix. Then we see

$$m_s^2 = 4v^2(1+\varepsilon')\lambda^2, \quad \text{with} \quad \varepsilon' = \frac{A_\lambda}{\mu\tan\beta} - 1, \tag{C3}$$

where $A_\lambda$ is the soft trilinear scalar coupling of Eq. (1). The corrections from mixing, however, can be of the same order. With the mixing corrections included, the tree-level saxion mass is given by

$$m_s^2 = -\frac{4(\lambda^2 v^2 \mu^2 \varepsilon'^2)}{m_Z^2} + \frac{4\lambda^2 v^2}{m_Z^6}\left(4v^2\varepsilon'^4\lambda^2\mu^4 + \frac{m_Z^4(1-\varepsilon')(m_Z^2+2\varepsilon'\mu^2)}{\tan^2\beta}\right) + \sum_i \mathcal{O}\left(\frac{\lambda^{5-i}}{\tan^i\beta}\right). \tag{C4}$$

At tree level, the first term is negative, while the second term is smaller than the first by a factor $\sum_i \mathcal{O}(\frac{\lambda^{2-i}}{\tan^i\beta})$. Thus, to avoid a tachyonic vacuum,

$$\varepsilon'^2 < \frac{m_Z^2}{\mu^2\tan^2\beta} \tag{C5}$$

is required [2]. This condition sets an upper bound for the tree-level $m_s^2$

$$m_s^2 < \frac{4v^2\lambda^2}{\tan^2\beta}, \tag{C6}$$

which is $(\mathcal{O}(10)\ \mathrm{GeV})^2$ or lower in the context we consider.

The $\mathcal{O}(10)$ GeV saxion mass feature can be seen in another way. It is easy to calculate the determinant of the mass squared matrix of the $CP$-even Higgs bosons, which is given by

$$\det M = -4\lambda^2 v^2 \tan\beta^2 \mu^4 (1+\varepsilon') \times \left(\varepsilon'^2 - \frac{m_Z^2(1-\varepsilon') - \varepsilon'(2+\varepsilon')\mu^2}{\mu^2\tan^2\beta}\right) + \sum_i \mathcal{O}\left(\frac{\lambda^{4-i}}{\tan^i\beta}\right). \tag{C7}$$

To avoid a tachyonic vacuum at tree level, the determinant must be positive, which immediately leads to the condition given in Eq. (C5) if $\varepsilon' > -1$.

We now address the question of why the saxion mass does not get a large mass correction from the soft SUSY breaking mass term of the singlet field, even though the saxion is singletlike. Recall the vacuum stability conditions are twofold. First, the Higgs potential must be locally flat at the vacuum point, so its first-order partial derivative with respect to the field variables must be zero. Second, the physical masses of the scalar particles cannot be negative, which implies that the second-order partial derivative with respect to the mass eigenstates must be positive. The latter has been discussed above via the determinant argument. To see what the former implies, we start by expressing the scalars as

$$H_u^0 = v_u + \frac{H_u^R + iH_u^I}{\sqrt{2}}, \quad H_d^0 = v_d + \frac{H_d^R + iH_d^I}{\sqrt{2}}, \quad S = v_S + \frac{S^R + iS^I}{\sqrt{2}}. \tag{C8}$$

We can derive the locally flat conditions for the $CP$-even Higgs components[3] and reexpress the soft SUSY-breaking Higgs masses in terms of $\lambda$, $A_\lambda$, $v_u$, $v_d$, and $v_S$. At tree level, they are given by

$$m_{H_d}^2 = -\mu^2 + B_\mu \tan\beta - \frac{m_Z^2}{2}\cos 2\beta, \quad m_{H_u}^2 = -\mu^2 + B_\mu \cot\beta + \frac{m_Z^2}{2}\cos 2\beta, \quad m_S^2 = -\lambda^2 v^2 + A_\lambda \lambda^2 v^2 \frac{\sin 2\beta}{2\mu}, \tag{C9}$$

where

$$B_\mu = \mu A_\lambda - \frac{\lambda^2 v^2 \sin 2\beta}{2}, \tag{C10}$$

and $\mu = \lambda v_S$ as usual. For $\tan^2\beta \gg 1$, the right hand side of Eq. (C9) can be expanded as

$$m_{H_d}^2 = \mu^2\tan^2\beta(1+\varepsilon') - \mu^2 - \lambda^2 v^2 + \frac{M_Z^2}{2} + \mathcal{O}\left(\frac{1}{\tan^2\beta}\right), \tag{C11}$$

$$m_{H_u}^2 = \mu^2\varepsilon' - \frac{M_Z^2}{2} + \mathcal{O}\left(\frac{1}{\tan^2\beta}\right), \tag{C12}$$

$$m_S^2 = \lambda^2 v^2 \varepsilon' + \mathcal{O}\left(\frac{1}{\tan^2\beta}\right). \tag{C13}$$

So, $m_S^2$ needs to be much smaller than the squared EW scale to get a stable vacuum. Thus, in the PQ symmetry limit, the vacuum stability forbids the saxion to obtain a large mass correction from softly SUSY breaking effects.

[3]In this article, we assume that there is neither explicit nor spontaneous $CP$ violation. In this case, the locally flat conditions with respect to $CP$-odd Higgs components are satisfied automatically.

[1] J. Huang, T. Liu, L.-T. Wang, and F. Yu, Phys. Rev. Lett. **112**, 221803 (2014).
[2] P. Draper, T. Liu, C. E. M. Wagner, L.-T. Wang, and H. Zhang, Phys. Rev. Lett. **106**, 121805 (2011).
[3] M. Bastero-Gil, C. Hugonie, S. F. King, D. P. Roy, and S. Vempati, Phys. Lett. B **489**, 359 (2000), and references therein; A. de Gouvea, A. Friedland, and H. Murayama, Phys. Rev. D **57**, 5676 (1998); J. R. Ellis, J. F. Gunion, H. E. Haber, L. Roszkowski, and F. Zwirner, Phys. Rev. D **39**, 844 (1989); S. W. Ham, S. K. Oh, and B. R. Kim, J. Phys. G **22**, 1575 (1996); D. J. Miller, R. Nevzorov, and P. M. Zerwas, Nucl. Phys. **B681**, 3 (2004).
[4] C. Panagiotakopoulos and K. Tamvakis, Phys. Lett. B **469**, 145 (1999).
[5] V. Barger, P. Langacker, H.-S. Lee, and G. Shaughnessy, Phys. Rev. D **73**, 115010 (2006).
[6] A. Arbey, M. Battaglia, and F. Mahmoudi, Eur. Phys. J. C **72**, 2169 (2012); E. Kuflik, A. Pierce, and K. M. Zurek, Phys. Rev. D **81**, 111701 (2010); D. Feldman, Z. Liu, and P. Nath, Phys. Rev. D **81**, 117701 (2010); C. Boehm, P. S. B. Dev, A. Mazumdar, and E. Pukartas, J. High Energy Phys. 06 (2013) 113; L. Calibbi, J. M. Lindert, T. Ota, and Y. Takanishi, J. High Energy Phys. 10 (2013) 132.
[7] S. Chatrchyan *et al.* (CMS Collaboration), Phys. Lett. B **716**, 30 (2012).
[8] G. Aad *et al.* (ATLAS Collaboration), Phys. Lett. B **716**, 1 (2012).
[9] L. Goodenough and D. Hooper, arXiv:0910.2998.
[10] D. Hooper and L. Goodenough, Phys. Lett. B **697**, 412 (2011).
[11] D. Hooper and T. Linden, Phys. Rev. D **84**, 123005 (2011).
[12] K. N. Abazajian and M. Kaplinghat, Phys. Rev. D **86**, 083511 (2012).
[13] D. Hooper, I. Cholis, T. Linden, J. Siegal-Gaskins, and T. Slatyer, Phys. Rev. D **88**, 083009 (2013).
[14] C. Gordon and O. Macias, Phys. Rev. D **88**, 083521 (2013).
[15] K. N. Abazajian, N. Canac, S. Horiuchi, and M. Kaplinghat, Phys. Rev. D **90**, 023526 (2014).
[16] T. Daylan, D. P. Finkbeiner, D. Hooper, T. Linden, S. K. N. Portillo, N. L. Rodd, and T. R. Slatyer, arXiv:1402.6703.
[17] V. Barger, Y. Gao, M. McCaskey, and G. Shaughnessy, Phys. Rev. D **82**, 095011 (2010).
[18] K. C. Y. Ng, R. Laha, S. Campbell, S. Horiuchi, B. Dasgupta, K. Murase, and J. F. Beacom, Phys. Rev. D **89**, 083001 (2014).
[19] N. Okada and O. Seto, Phys. Rev. D **89**, 043525 (2014).
[20] K. P. Modak, D. Majumdar, and S. Rakshit, arXiv:1312.7488.
[21] C. Boehm, M. J. Dolan, C. McCabe, M. Spannowsky, and C. J. Wallace, J. Cosmol. Astropart. Phys. 05 (2014) 009.
[22] E. Hardy, R. Lasenby, and J. Unwin, J. High Energy Phys. 07 (2014) 049.
[23] D. P. Finkbeiner and N. Weiner, arXiv:1402.6671.
[24] A. Alves, S. Profumo, F. S. Queiroz, and W. Shepherd, arXiv:1403.5027.
[25] A. Berlin, D. Hooper, and S. D. McDermott, Phys. Rev. D **89**, 115022 (2014).
[26] P. Agrawal, B. Batell, D. Hooper, and T. Lin, Phys. Rev. D **90**, 063512 (2014).
[27] E. Izaguirre, G. Krnjaic, and B. Shuve, Phys. Rev. D **90**, 055002 (2014).
[28] D. G. Cerdeno, M. Peiro, and S. Robles, J. Cosmol. Astropart. Phys. 08 (2014) 005.
[29] S. Ipek, D. McKeen, and A. E. Nelson, Phys. Rev. D **90**, 055021 (2014).
[30] K. Kong and J.-C. Park, Nucl. Phys. **B888**, 154 (2014).
[31] P. Ko, W.-I. Park, and Y. Tang, J. Cosmol. Astropart. Phys. 09 (2014) 013.
[32] C. Boehm, M. J. Dolan, and C. McCabe, Phys. Rev. D **90**, 023531 (2014).
[33] M. Abdullah, A. DiFranzo, A. Rajaraman, T. M. P. Tait, P. Tanedo, and A. M. Wijangco, Phys. Rev. D **90**, 035004 (2014).
[34] D. K. Ghosh, S. Mondal, and I. Saha, arXiv:1405.0206.
[35] A. Martin, J. Shelton, and J. Unwin, arXiv:1405.0272 [Phys. Rev. D (to be published)].
[36] A. Berlin, P. Gratia, D. Hooper, and S. D. McDermott, Phys. Rev. D **90**, 015032 (2014).
[37] T. Basak and T. Mondal, arXiv:1405.4877.
[38] J. M. Cline, G. Dupuis, Z. Liu, and W. Xue, J. High Energy Phys. 08 (2014) 131.
[39] W. Detmold, M. McCullough, and A. Pochinsky, arXiv:1406.2276.
[40] L. Wang, arXiv:1406.3598.
[41] B. D. Fields, S. L. Shapiro, and J. Shelton, Phys. Rev. Lett. **113**, 151302 (2014).
[42] C. Arina, E. Del Nobile, and P. Panci, arXiv:1406.5542.
[43] S. D. McDermott, arXiv:1406.6408.
[44] E. Carlson and S. Profumo, Phys. Rev. D **90**, 023015 (2014).
[45] T. Bringmann, M. Vollmann, and C. Weniger, arXiv:1406.6027 [Phys. Rev. D (to be published)].
[46] A. Djouadi and G. Moreau, Eur. Phys. J. C **73**, 2512 (2013).
[47] J. Shu and Y. Zhang, Phys. Rev. Lett. **111**, 091801 (2013).
[48] K. Tamvakis and D. Wyler, Phys. Lett. **112B**, 451 (1982); J. F. Nieves, Phys. Rev. D **33**, 1762 (1986); B. Bellazzini, C. Csaki, J. Hubisz, J. Shao, and P. Tanedo, J. High Energy Phys. 09 (2011) 035.
[49] D. J. Miller, S. Moretti, and R. Nevzorov, arXiv:hep-ph/0501139.
[50] A. Menon, D. E. Morrissey, and C. E. M. Wagner, Phys. Rev. D **70**, 035005 (2004).
[51] V. Barger, P. Langacker, and H.-S. Lee, Phys. Lett. B **630**, 85 (2005).
[52] R. Agnese *et al.* (SuperCDMSSoudan Collaboration), Phys. Rev. Lett. **112**, 041302 (2014).
[53] J. Angle *et al.* (XENON10 Collaboration), Phys. Rev. Lett. **107**, 051301 (2011).
[54] E. Aprile *et al.* (XENON100 Collaboration), Phys. Rev. Lett. **109**, 181301 (2012).
[55] D. S. Akerib *et al.* (LUX Collaboration), Phys. Rev. Lett. **112**, 091303 (2014).
[56] C. E. Aalseth *et al.* (CoGeNT Collaboration), Phys. Rev. D **88**, 012002 (2013).
[57] R. Bernabei *et al.* (DAMA and LIBRA Collaborations), Eur. Phys. J. C **67**, 39 (2010).
[58] G. Angloher *et al.*, Eur. Phys. J. C **72**, 1971 (2012).
[59] R. Agnese *et al.* (CDMS Collaboration]) Phys. Rev. Lett. **111**, 251301 (2013).

[60] A. Bottino, N. Fornengo, and S. Scopel, Phys. Rev. D **67**, 063519 (2003); J. F. Gunion, D. Hooper, and B. McElrath, Phys. Rev. D **73**, 015011 (2006); F. Petriello and K. M. Zurek, J. High Energy Phys. 09 (2008) 047; J. Kopp, T. Schwetz, and J. Zupan, J. Cosmol. Astropart. Phys. 02 (2010) 014; A. L. Fitzpatrick, D. Hooper, and K. M. Zurek, Phys. Rev. D **81**, 115005 (2010); S. Andreas, C. Arina, T. Hambye, F.-S. Ling, and M. H. G. Tytgat, Phys. Rev. D **82**, 043522 (2010); S. Chang, J. Liu, A. Pierce, N. Weiner, and I. Yavin, J. Cosmol. Astropart. Phys. 08 (2010) 018; K. J. Bae, H. D. Kim, and S. Shin, Phys. Rev. D **82**, 115014 (2010); D. Hooper, J. I. Collar, J. Hall, D. McKinsey, and C. Kelso, Phys. Rev. D **82**, 123509 (2010); D. Das and U. Ellwanger, J. High Energy Phys. 09 (2010) 085; M. R. Buckley, D. Hooper, and T. M. P. Tait, Phys. Lett. B **702**, 216 (2011); D. Hooper, N. Weiner, and W. Xue, Phys. Rev. D **86**, 056009 (2012); R. C. Cotta, A. Rajaraman, T. M. P. Tait, and A. M. Wijangco, Phys. Rev. D **90**, 013020 (2014); J. Cao, C. Han, L. Wu, P. Wu, and J. M. Yang, J. High Energy Phys. 05 (2014) 056.

[61] J.-J. Cao, K.-i. Hikasa, W. Wang, J. M. Yang, K.-i. Hikasa, W.-Y. Wang, and J. M. Yang, Phys. Lett. B **703**, 292 (2011); J. Kozaczuk and S. Profumo, Phys. Rev. D **89**, 095012 (2014); D. A. Vasquez, G. Belanger, C. Boehm, A. Pukhov, and J. Silk, Phys. Rev. D **82**, 115027 (2010); D. Albornoz Vasquez, G. Belanger, and C. Boehm, Phys. Rev. D **84**, 095008 (2011); B. Bellazzini, C. Csaki, J. Hubisz, J. Shao, and P. Tanedo, J. High Energy Phys. 09 (2011) 035; D. G. Cerdeno, T. Delahaye, and J. Lavalle, Nucl. Phys. **B854**, 738 (2012).

[62] K. Griest and D. Seckel, Phys. Rev. D **43**, 3191 (1991).

[63] P. Gondolo and G. Gelmini, Nucl. Phys. **B360**, 145 (1991).

[64] W.-L. Guo and Y.-L. Wu, Phys. Rev. D **79**, 055012 (2009).

[65] B. A. Dobrescu, G. L. Landsberg, and K. T. Matchev, Phys. Rev. D **63**, 075003 (2001); B. A. Dobrescu and K. T. Matchev, J. High Energy Phys. 09 (2000) 031; R. Dermisek and J. F. Gunion, Phys. Rev. Lett. **95**, 041801 (2005); S. Chang, P. J. Fox, and N. Weiner, J. High Energy Phys. 08 (2006) 068; P. W. Graham, A. Pierce, and J. G. Wacker, arXiv:hep-ph/0605162.

[66] D. Curtin *et al.*, Phys. Rev. D **90**, 075004 (2014).

[67] S. Chang and N. Weiner, J. High Energy Phys. 05 (2008) 074.

[68] J. Goodman, M. Ibe, A. Rajaraman, W. Shepherd, T. M. P. Tait, and H.-B. Yu, Phys. Lett. B **695**, 185 (2011); Y. Bai, P. J. Fox, and R. Harnik, J. High Energy Phys. 12 (2010) 048; A. Rajaraman, W. Shepherd, T. M. P. Tait, and A. M. Wijangco, Phys. Rev. D **84**, 095013 (2011).

[69] U. Ellwanger, J. F. Gunion, and C. Hugonie, J. High Energy Phys. 02 (2005) 066; U. Ellwanger and C. Hugonie, Comput. Phys. Commun. **175**, 290 (2006); G. Belanger, F. Boudjema, C. Hugonie, A. Pukhov, and A. Semenov, J. Cosmol. Astropart. Phys. 09 (2005) 001; U. Ellwanger and C. Hugonie, Comput. Phys. Commun. **177**, 399 (2007); M. Muhlleitner, A. Djouadi, and Y. Mambrini, Comput. Phys. Commun. **168**, 46 (2005); D. Das, U. Ellwanger, and A. M. Teixeira, Comput. Phys. Commun. **183**, 774 (2012).

[70] ATLAS Collaboration, Report No. ATLAS-CONF-2013-034; CMS Collaboration, Report No. CMS-PAS-HIG-13-005; G. Belanger, B. Dumont, U. Ellwanger, J. F. Gunion, and S. Kraml, Phys. Lett. B **723**, 340 (2013); P. P. Giardino, K. Kannike, I. Masina, M. Raidal, and A. Strumia, J. High Energy Phys. 05 (2014) 046; J. Cao, F. Ding, C. Han, J. M. Yang, and J. Zhu, J. High Energy Phys. 11 (2013) 018.

[71] D. Alves *et al.* (LHC New Physics Working Group Collaboration), J. Phys. G **39**, 105005 (2012).

[72] F. Yu, Phys. Rev. D **90**, 015009 (2014).

[73] J. Alwall, M. Herquet, F. Maltoni, O. Mattelaer, and T. Stelzer, J. High Energy Phys. 06 (2011) 128.

[74] J. Pumplin, D. R. Stump, J. Huston, H. L. Lai, P. M. Nadolsky, and W. K. Tung, J. High Energy Phys. 07 (2002) 012.

[75] M. L. Mangano, M. Moretti, and R. Pittau, Nucl. Phys. **B632**, 343 (2002).

[76] M. L. Mangano, M. Moretti, F. Piccinini, R. Pittau, and A. D. Polosa, J. High Energy Phys. 07 (2003) 001.

[77] T. Sjostrand, S. Mrenna, and P. Z. Skands, J. High Energy Phys. 05 (2006) 026.

[78] M. Cacciari, G. P. Salam, and G. Soyez, Eur. Phys. J. C **72**, 1896 (2012).

[79] S. Chatrchyan *et al.* (CMS Collaboration), JINST **6**, P11002 (2011).

[80] G. Aad *et al.* (ATLAS Collaboration), Eur. Phys. J. C **72**, 1909 (2012).

[81] ATLAS Collaboration, Report No. ATLAS-CONF-2011-063.

[82] S. Chatrchyan *et al.* (CMS Collaboration), JINST **6**, P09001 (2011).

[83] R. Bonciani, S. Catani, M. L. Mangano, and P. Nason, Nucl. Phys. **B529**, 424 (1998); **B803**, 234(E) (2008).

[84] S. Heinemeyer *et al.* (LHC Higgs Cross Section Working Group Collaboration), arXiv:1307.1347.

[85] Y. L. Dokshitzer, G. D. Leder, S. Moretti, and B. R. Webber, J. High Energy Phys. 08 (1997) 001.

[86] M. Wobisch and T. Wengler, in *Proceedings of the Workshop on Monte Carlo Generators for HERA Physics, Hamburg, 1998/1999*, pp. 270–279.

[87] T. Han, Z. Liu, and S. Su, J. High Energy Phys. 08 (2014) 093.

[88] C. Cheung, M. Papucci, D. Sanford, N. R. Shah, and K. M. Zurek, Phys. Rev. D **90**, 075011 (2014).